lajss.org© Latin American Journal of Solids and Structures

www.lajss.org

Verification of a material model and estimation of the friction coefficient on the contouring of Ti rods

Arthur Sanchez de Almeida[a*], Carlos Rodrigo de Mello Roesler[b], Arthur Paiva Grimaldi Santos[a]

[a] Biomechanical Engineering Laboratory, Federal University of Santa Catarina, Florianópolis, SC, Brazil. Email: arthur.almeida@outlook.com, arthur.pgsantos@gmail.com

[b] Department of Mechanical Engineering, Federal University of Santa Catarina, Florianópolis, SC, Brazil. Email: r.roesler@ufsc.br

* Corresponding author

Abstract

This study explores the efficacy of 2D Digital Image Correlation (DIC) for material characterization of titanium spinal rods, particularly under large strain conditions. The research aims to address the lack of comprehensive material data by performing tensile tests of cylindrical specimens and applying 2D digital image correlation to derive the true stress-strain curve during plastic deformation, assuming negligible out-of-plane displacements and adopting Gromada's coefficient of correction for triaxial stress state. The verification process includes a direct comparison with available manufacturer and literature specifications, as well as an experimental four-point bending test in conjunction with a numerical model for comparative analysis. Results demonstrate that 2D DIC, with adjustments for triaxial stress states, can reliably determine material properties, showing less than 5% deviation from established literature values. The findings advocate for the cost-effective use of 2D DIC as a promising tool for enhancing the accuracy of finite element models, especially in applications involving large deformation.

Keywords

Experimental material properties, digital image correlation (DIC), finite element model, tensile test

Graphical Abstract

1 INTRODUCTION

A crucial step in developing a finite element model representing forming operations is to obtain accurate properties of the materials being represented, especially the determination of the stress-strain relationship up to large strains. Since manufacturer specifications usually do not encompass the true stress-strain curve under plastic deformations, performing a tensile test is essential to ascertain these parameters with confidence. Assessing the actual strain using extensometers attached to the test specimens can be a challenging process; instead, images can be captured aiming at the application of the Digital Image Correlation (DIC) method.

In the case of a cylindrical test specimen, a complex stereo (3D) DIC setup is usually recommended. However, while stereo DIC offers enhanced capabilities that are indispensable for a range of specialized application, the two-dimensional (2D) technique has the advantage of requiring only a single camera, thus minimizing the costs of equipment and simplifying the experimental apparatus. Furthermore, two-dimensional process eliminates the need for complex calibration procedures, reducing both time and knowledge demanded for material characterization. Although, this approach has the disadvantage of requiring all displacements to occur within the measurement plane or else an error in the results will be generated.

The DIC method has been developed since the early 1980s. Zhao, Sang and Duan (2019) summarizes how the result of several advances has led to the efficiency and measurement accuracy of algorithms being significantly improved in recent years, allowing the popularization and applications of the method in previously impractical situations. Therefore, the aim of this study is to investigate the use of 2D DIC, with corrections for triaxial stresses, as a cost-effective and reliable method compared to stereo DIC for determining material properties in finite element analysis. This could lead to more accurate and economical modeling in medical device development.

2 MATERIAL AND METHODS

The methodology employed in this study is structured into two major phases. Initially, a tensile test adhering to the ASTM International (2022) E8/E8M standard guidelines was conducted while employing digital image correlation techniques to capture the post-necking behavior of the material, allowing the implementation of the triaxial stress state correction method presented by Gromada, Mishuris, and Öchsner (2011) to obtain the equivalent stress-strain curve. Upon determining the material properties, the study advances to a verification phase, where the plastic behavior of the rods is assessed. This is achieved through comparation between a four-point flexure test and a corresponding numerical model, incorporating the material properties ascertained from the tensile test.

2.1 Tensile test: Experimental setup and data manipulation

Four (n = 4) rigid spinal rods made of Ti Grade 2 were machined to produce cylindrical dog bone specimens with a diameter of 4.0 mm and a parallel length of 24.0 mm. The specimens underwent traction testing using a Shimadzu Autograph AGS-X 100kN universal machine at a displacement rate of 1 mm/min until failure.

In order to infer the real stresses, images of the test were captured for the application of DIC method, one of the key principles of this optical measurement method is the application of a speckle pattern to the specimen's surface. Since the specimens do not exhibit super-elasticity characteristics or have surfaces where paint does not adhere, patterns of satisfactory quality were achieved by spraying paint on the body's surface, as depicted in Figure 1. To prevent the specimen from slipping in the machine's attachment, the extremities outside the region of interest were left unpainted.

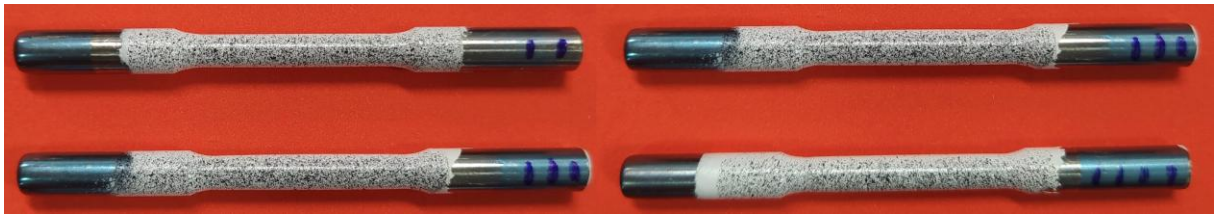

Figure 1: Specimens with speckle pattern applied

The tensile test images were captured using a Point Grey Research, Inc. FL2G-13S2M-C 1394 camera, which features a Sony ICX445 CCD sensor. The camera settings were configured to record at a rate of 8 frames per second, with an image resolution of 1288 × 964 pixels. Figure 2 depicts the tensile test's experimental arrangement and provides a representative sample from the image sequence obtained.

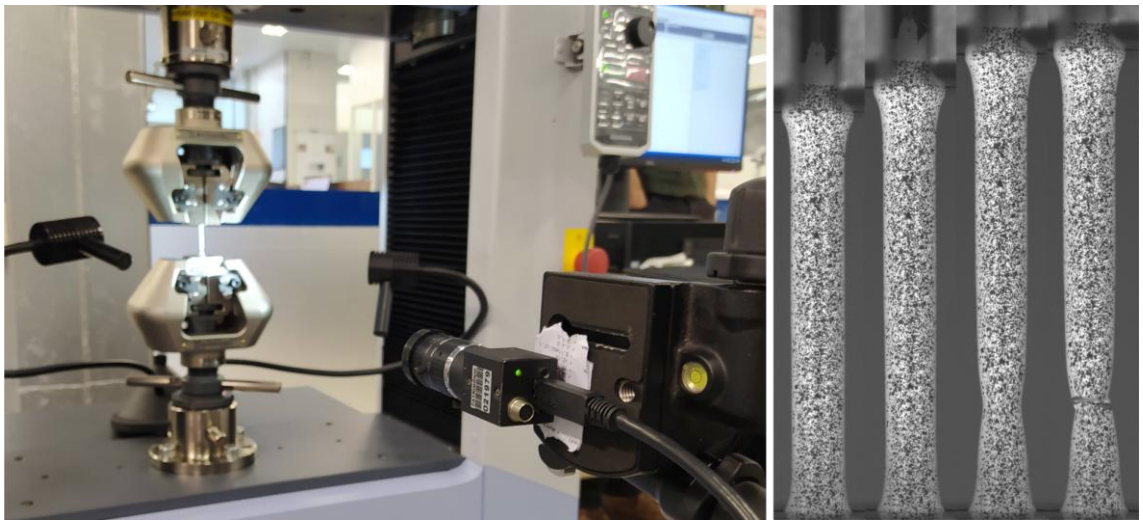

Figure 2: Experimental apparatus during test (left) and sample from the images obtained (right)

After the acquisition of the images, the data processing stage begins. The Ncorr v1.1.2 software and the Ncorr Post v2.0 plugin were used at this stage of the study. The workflow is summarized as follows: loading the pictures and defining the reference image, defining the region of interest and the parameters of the algorithm, performing the correlation calculations, and finally formatting the displacements and strain. Blaber and Antoniou (2015) advise that, among the parameters of the algorithm, the radius of the subsets has the greatest impact. Generally, the main idea is to define the smallest possible subset that does not result in excessively noise data. In this work, after a few iterations, a radius of 18 pixels was chosen.

Since all procedures adopt pixels as a unit of distance, a theoretical transformation is necessary to convert pixels into spatial units. For 2D algorithms, this procedure is based on a single scale factor, and small errors in its determination can be intensified in subsequent steps, hence the use of a precision reference is encouraged. A Dino-Lite calibration ruler with a resolution of 0.2 mm has been introduced in the scene corresponding to the reference image, as shown in Figure 3, and the processing results are scaled from a distance measured on this ruler.

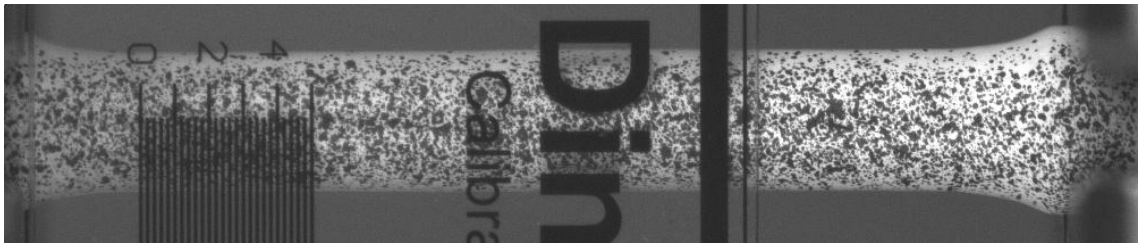

Figure 3: Calibration ruler superimposed on the specimen

After calculating the displacement field, the data are imported into the Ncorr Post v2.0 plug-in, which enables the acquisition of results along a pre-defined line, a technique known as virtual extensometer. The analysis aims to determine the real stress during the test, therefore two extensometers, positioned as shown in Figure 4, are necessary: the first tracks the axial elongation of the specimen at an initial length of 24 mm, while the second is associated with the diameter at the critical section where rupture occurs. The creation of the virtual extensometer requires the user to define the start (a) and end (b) points.

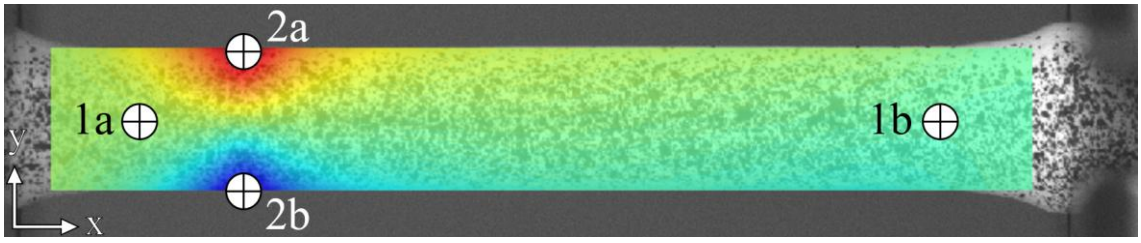

Figure 4: Positioning of axial and diametral extensometers

For application of the two-dimensional method to a cylindrical specimen, it is assumed that displacements outside the plane of the virtual extensometer are negligible. The instantaneous diameter of the specimen, D_i, is calculated by Eq. (1).

$$D_i = D_0(1 + \Delta_D) \tag{1}$$

Where D_0 is the initial diameter and Δ_D represents the displacement values from the diametral extensometer. This conversion is intended to correct any discrepancies caused by the photographic capture of the diameter not being in the same plane as the calibration ruler. Finally, the initial diameter, D_0, of the useful parallel section is determined through a process in which each specimen undergoes three measurements, equally spaced along its length, using a micrometer. Subsequently, the specimen is rotated 90 degrees, and three additional measurements are taken. Table 1 presents the average values obtained for each test specimen (S).

Table 1 Experimental specimen initial diameter, $\mathrm{D_0}$, measurements.

	S1	S2	S3	S4
$\mathrm{D_0}$ (mm)	4.07 ± 0.02	3.99 ± 0.01	4.24 ± 0.01	4.27 ± 0.01

After conducting the tensile tests and processing the images, the elongation data from the virtual extensometers, along with the force measured by the load cell, are imported into a custom Matlab routine. This routine generates the corrected real stress-strain curve necessary for defining a material model in finite element software.

Initially, the start and end points of the tests are manually identified to exclude data post-rupture and prior to force application. Temporal smoothing is then applied to mitigate noise using a moving average filter with a 12-interval window and linear approximation, the relevance of this procedure is documented in studies such as Pan et al. (2008) and Castro (2012) as cited in Pinto (2014). Following the smoothing process, the values are interpolated onto a uniform time vector.

With the processed data, the transformation from force and displacement to engineering stress, σ_e, and strain, ε_e, is performed using standard equations. From the engineering stress-strain curve, certain material properties can be deduced. Young's Modulus, E, being the slope of the curve's linear segment, is obtained from the linear regression of the elastic region, ranging from 10% to 50% of the test's maximum strength, as per ABNT (2013) NBR ISO 6892-1 guidelines.

Since the exact yield point of the curve is not always obvious, the yield stress, σ_y, is determined at the intersection of a line offset by 0.2% from the linear elastic region and the stress-strain curve, as recommended by the respective NBR ISO. Subsequently, the tensile strength, σ_u, is also determined. However, the engineering approach is known for not accounting for the instantaneous dimensions of the component during testing. That said, theoretical real stress and strain can be expressed through engineering values with the aid of Eq. (2) and Eq. (3).

$$\varepsilon = \ln(1 + \varepsilon_e) \tag{2}$$

$$\sigma = \sigma_e(1 + \varepsilon_e) \tag{3}$$

Beyond the maximum load point, real stress should be determined by experimental measurements of the cross-sectional area. Let A the instantaneous minimum section area and admitting that the specimen cross section remains circular for the entire duration of the test, the actual stress and strain after the onset of necking can be expressed by Eq. (4) and Eq. (5).

$$\varepsilon_{DIC} = \ln\left(\frac{A_0}{A}\right) = \ln\frac{(\pi/4)D_0^2}{(\pi/4)D_i^2} = 2\ln\left(\frac{D_0}{D_i}\right) \tag{4}$$

$$\sigma_{DIC} = \frac{\mathrm{F}}{A} = \frac{\mathrm{F}}{(\pi/4)D_i^2} = \frac{4\mathrm{F}}{\pi D_i^2} \tag{5}$$

After the onset of necking, the strain is localized in the diameter-reduced zone, accompanied by the development of a triaxial stress state (Bridgman, 1943). Generally, for a known correction factor, ζ, and mean axial stress, σ_{DIC}, the corrected equivalent stress, σ_{eq}, can be calculated from Eq. (6)

$$\sigma_{eq} = \zeta\, \sigma_{DIC} \tag{6}$$

More recently, the correction coefficient proposed by Gromada, Mishuris, and Öchsner (2011), presented in Eq. (7) where γ e β, are experimental calibration coefficients, has gained recognition for its effectiveness. (Tu et al., 2020)

$$\zeta = 1 + \frac{a}{4R} + \frac{a(1-\beta)\gamma}{4R(4-\gamma)} \tag{7}$$

Gromada, Mishuris, and Öchsner (2011) asserts that by adopting $\gamma = \beta = 0.5$, Eq. (6) becomes more straightforward and still yield acceptable accuracy. It is evident from the equation that precise experimental measurement of the a/R parameter, where a is the minimum cross-sectional radius and R the curvature radius of necking, is essential for satisfactory results. However, the experimental measurement of these values is complex and time-consuming. Le Roy et al. (1981) proposes a relationship for calculating the ratio a/R expressed in terms of current axial deformation, ε_{DIC}, and deformation at the onset of necking, ε_{est} by the Eq. (8). With ε_{DIC} and σ_{eq} defined is possible to express the real stress-strain curve of the material.

$$\frac{a}{R} = 1{,}1\ (\varepsilon_{DIC} - \varepsilon_{est}) \tag{8}$$

2.1 Method Verification: Flexural test and Finite Element model

Once the material properties have been obtained, it is necessary to verify the accuracy of the adopted procedure, which implies verifying the initial assumptions made for the application of two-dimensional digital image correlation. Specifically, whether the hypothesis that out-of-plane displacements minimally impact the measurements of a virtual extensometer positioned on the axial axis of the specimen and the diameter measurements are valid.

The flexure test, when employed as a reference, facilitates the assessment of the material model's fidelity. The test was standardized in accordance with the ASTM International (2020) F2193-20, which delineates the protocol for evaluating rods used in spinal fixation systems. The experimental configuration adopted for this test is depicted in Fig 5.

The tests were carried out on an EMIC universal testing machine, model DL3000, with the attachments adjusted so that the distance between the supports is 60 mm, and the distance between the two load application points, as well as the distance between the load application point and the nearest support, is 20 mm. The load-bearing rollers used are 12 mm in diameter with a V-shaped notch at the midpoint of their length to accommodate the rod. Under displacement control, the tests were performed at a rate of 5 mm/min until the maximum force point was reached. A total of two specimens were used (n = 2).

To analyze the plastic behavior of the rod the test configuration was numerically modeled using Ansys Mechanical 2020 R1. Figure 6 illustrates the boundary conditions applied in the analysis. By taking advantage of the inherent symmetry of the study, the model simplifies the setup geometry to a quarter-section using a XY and YZ planes for symmetry. The distance between the upper roller (loading) and the symmetry plane was set to 10 mm, while the distance between the lower roller (support) and the same plane was set to 30 mm, to mimic the experimental setup.

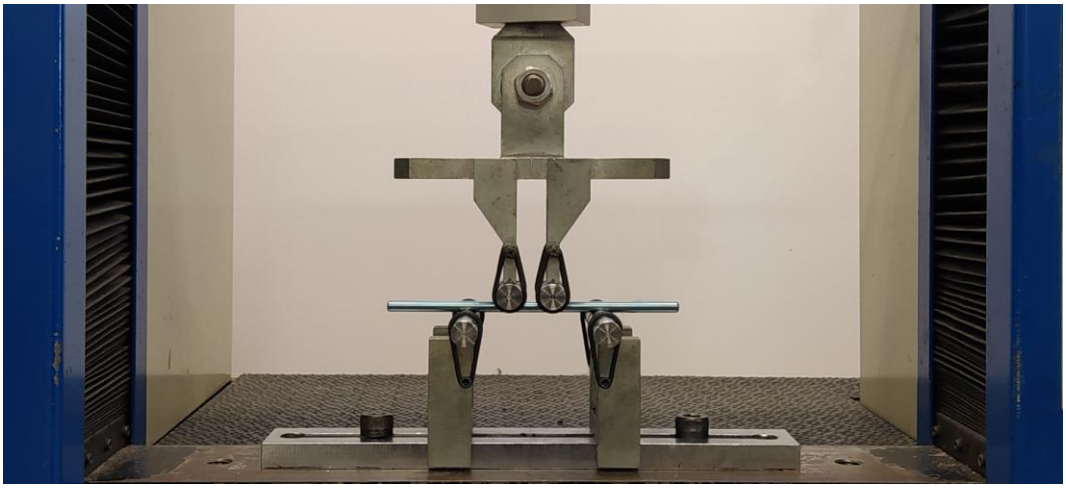

Figure 5: Experimental setup for four-point flexural test

During the analysis, the support roller is constrained ($\Delta S = 0$) in all directions by imposing zero nodal displacements on the horizontal cross section. Similarly, the displacements in the x and z directions are fixed on the load application rollers ($\Delta S_x = \Delta S_z = 0$). However, the loading roller is free to move along the y direction, where a vertical load (F_y) of -450 N is applied to the cross section. It should be noted that, due to symmetry conditions, the force in the numerical model is a quarter of that intended to be represented. To ensure convergence of the numerical model, the force was incrementally applied in steps of -5 N until reaching -25 N, and then in increments of -47.5 N until reaching -450 N.

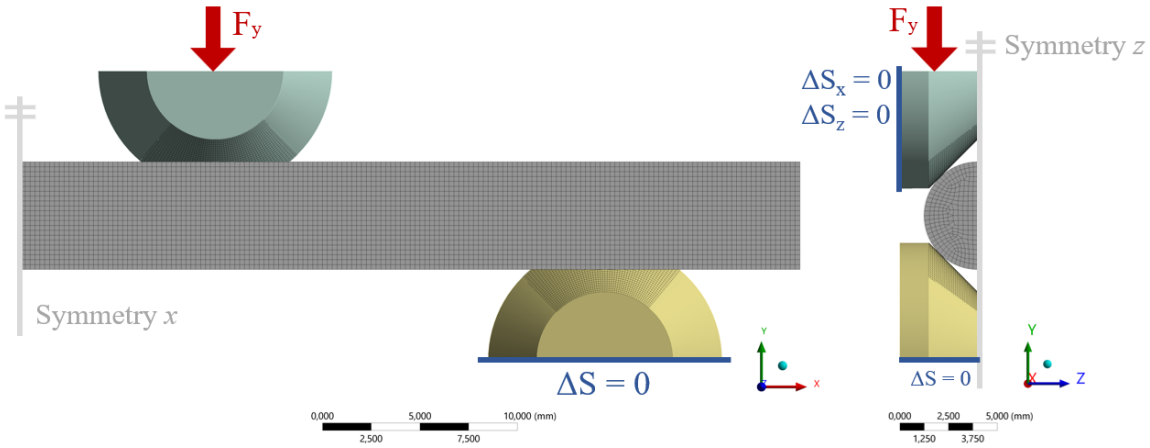

Figure 6: Numerical model representing the flexural test

The rollers are treated as idealized structures and set as rigid bodies, consequently a material model is not required. The rod material is characterized by a multilinear kinematic hardening plasticity model defined by a Young's modulus of 1.05×10^5 MPa, a Poisson's ratio of 0.34, and a stress-plastic strain curve described by the 25 data points (n) in Table 2.

Table 2 Data points for the plasticity model's input curve.

n	P. Strain (mm^{-1})	Stress (MPa)	*n*	P. Strain (mm^{-1})	Stress (MPa)	*n*	P. Strain (mm^{-1})	Stress (MPa)	*n*	P. Strain (mm^{-1})	Stress (MPa)	*n*	P. Strain (mm^{-1})	Stress (MPa)
1	0.0000	285.81	6	0.0146	484.76	11	0.0470	544.57	16	0.1195	594.90	21	0.2812	647.87
2	0.0021	386.05	7	0.0192	498.52	12	0.0573	554.96	17	0.1424	604.72	22	0.3322	659.07
3	0.0045	425.79	8	0.0245	511.05	13	0.0693	565.12	18	0.1692	614.47	23	0.3921	669.37
4	0.0073	450.44	9	0.0309	522.76	14	0.0835	575.14	19	0.2007	625.23	24	0.4624	679.06
5	0.0106	469.15	10	0.0383	533.88	15	0.1000	585.05	20	0.2377	636.42	25	0.5450	687.17

All components of the model were discretized with hexahedral elements. The average element size was set at 0.25 mm, determined by mesh sensitivity analysis as shown on Figure 7, where convergence was achieved with approximately 6% difference in the results of contact pressure between rod and support roller, and maximum principal stress on the rod over subsequent refinements. The mesh independence study was conducted with a coefficient of friction of 0.1 applied to the contacting surfaces.

As we increased the number of elements (i.e., decrease the element size), the solution converges to a stable and consistent result, with approximately 6% change on the contact pressure between a mesh size of 0.5 mm (5078 elements) and 0.25 mm (40784 elements). Convergence suggests that our model captures the essential physics and further mesh refinement does not significantly alter the results, but greatly increase the computational cost.

Finally, the contact between the rod and the rollers is defined by a Coulomb friction model with an augmented Lagrange algorithm to penalize penetrations. The procedure for obtaining the coefficient of friction, μ, was performed iteratively, testing values between 0 and 0.15 in increments of 0.05, to select the coefficient that best matched the numerical and experimental responses.

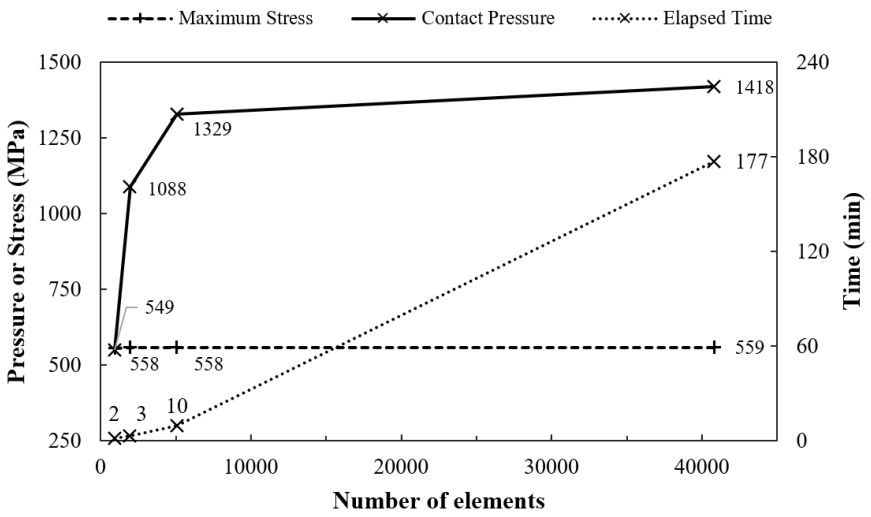

Figure 7: Mesh independence study

3 RESULTS

We do not intend to guide the way you want to write your paper, but a section RESULTS is nearly always present in all the papers, despite of having different names. We quote now Figure 2, fol-lowed by Table 1, where you should pay attention to the various format features.

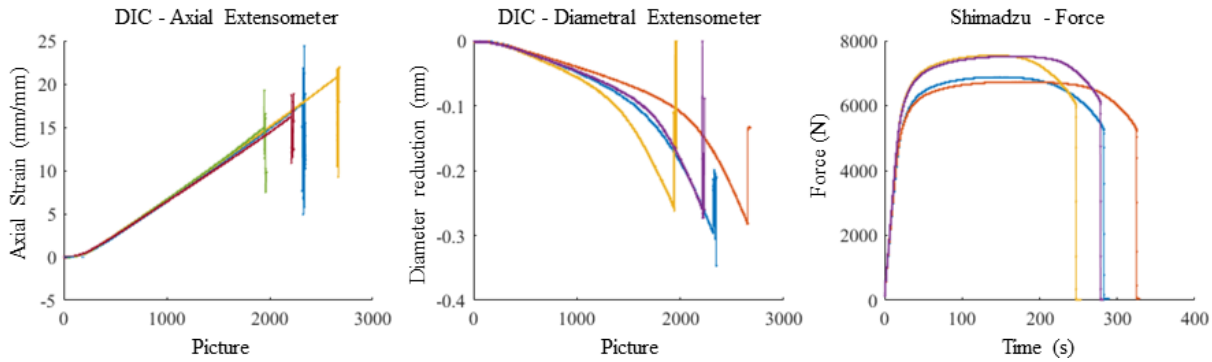

Figure 8: Raw data curves resulting from the tensile test

The raw data represented in these graphs are crucial for evaluating the DIC data generation process, including the assessment of noise levels and identification of potential outliers. Following the data manipulation procedures outlined in the methods section, the average values for the material's Young's modulus (E), yield stress (σ_y), yield strain (ε_y), ultimate stress (σ_u) and ultimate strain (ε_u) were computed. Table 3 provides a summary of the engineering properties for the tested material.

Table 3 Summary of engineering mechanical properties obtained for each specimen and average.

		S1	S2	S3	S4	Avg ± SD
E	(GPa)	103.07	107.90	110.44	99.59	105 ± 4
σ_y	(MPa)	407.90	412.65	412.81	404.54	409 ± 4
ε_y	(%)	0.60	0.58	0.57	0.61	0.59 ± 0.02
σ_u	(MPa)	528.37	536.65	533.17	523.05	530 ± 5
ε_u	(%)	8.31	10.43	7.76	8.73	8.80 ± 1

After the application of the described methods for deriving real values, the experimental stress-strain curves were generated as illustrated in Figure 9. It is important to observe that the elastic region appears compressed along the vertical axis due to considerable strain levels. Consistent with expectations, the real stress is plotted to the left of the

engineering curve up to the point of maximum loading, beyond which the experimental strain values significantly surpass the theoretical predictions.

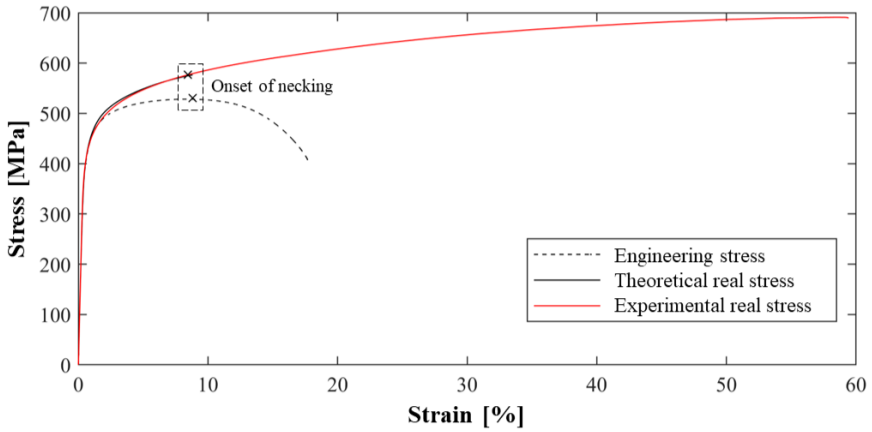

Figure 9: Strain-stress curves obtained for the material

After applying the material properties into the finite element model, the achieved force-displacement curves corresponding to each tested coefficient of friction were set against the experimental results, as depicted in Figure 10. Considering the comparative analysis, a coefficient of friction value of 0.1 was identified as providing the optimal alignment between the numerical and experimental curves.

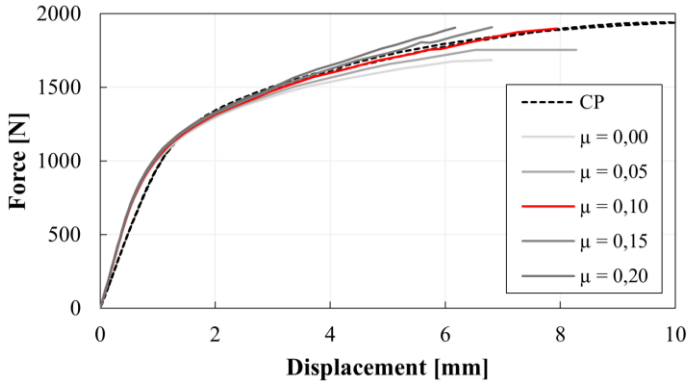

Figure 10: Numerical model response to different friction coefficients

4 DISCUSSION

Once the material properties have been obtained, it is necessary to verify the accuracy of the adopted procedure, which involves verifying the initial assumptions made for the application of two dimensional DIC. Specifically, it must be confirmed whether the hypothesis that distortions due to out-of-plane displacements have a negligible impact on the measurements taken by a virtual extensometer positioned along the axial axis of the specimen, as well as on the diameter measurements, holds true.

The results obtained were compared with those found in the literature, as shown in Table 4. The reference value for the modulus of elasticity can be found in the ASM Handbook Volume 23 (Narayan, 2012), while the yield strength and tensile strength values are provided by the material quality certificate supplied by the manufacturer of the rods used.

Table 4 Deviation of mechanical properties obtained and reference values.

		Experimental	Literature	% Deviation
E	(GPa)	105 ± 4	102.7	2.2
σ_y	(MPa)	409 ± 4	401.0	2.0
ε_u	(%)	530 ± 3	536.0	1.1

Thus, with deviation values lower than 5%, it is valid to state that the results obtained are satisfactory, providing confidence in the application of this material model in numerical simulations for further studies.

The congruence between the experimental results and the computational model serves a dual purpose: it verifies the material properties and enables the estimation of the friction coefficient (μ). This coefficient is crucial for accurately modeling the interactions between the force application points, the rod, and the supports in the laboratory setting. Precise determination of this coefficient is essential for the accurate representation of boundary conditions in subsequent numerical models. The value obtained is on the same scale of magnitude as the coefficient of 0.175 used by Berti et al. (2018). In this sense, the conformity between numerical and experimental results reiterates the material model's ability to satisfactorily represent the plastic behavior of the rods.

Comparing the results of the experimental and numerical model, more rigidity is noticeable on elastic behavior of the numerical model. More detailed investigations could provide insights into the origin of this discrepancy, making the model even more representative. Since the primary objective of this work is the subsequent use of the data in models with large deformations, the study of elastic behavior was not extensively pursued.

Some limitations must be acknowledged. Given that in the elastic regime, the displacement value is small, the accuracy of the DIC method may be compromised and is better suited for large strain models. Additionally, the study assumes that out-of-plane displacements during tensile testing are negligible. This assumption may not hold true for all testing conditions and could introduce errors in the stress-strain data if significant out-of-plane movements occur, mainly due to poor positioning of the test setup.

Research aimed at quantifying the impact of out-of-plane displacements on the accuracy of 2D DIC measurements and a methodology for determination of experimental coefficients for individual cases, as seen in Lu et al. (2021), would be valuable. This could further enhance the method's precision and help establish it as a standard practice for improve accuracy of finite element models. It is noteworthy that the proposed methodology might be refined and lead to the development of testing protocols to ensure consistency across different research groups.

4 CONCLUSION

For characterizing titanium spinal rods under large strain conditions, the 2D Digital Image Correlation method, in conjunction with techniques to account for triaxial stress state induced by necking, has proven to be capable of accurately determining the material properties from a dog bone specimen subjected to a tensile test. Furthermore, when used alongside a finite element model, these material properties play a crucial role in estimating the friction coefficient within an experimental setup by selecting the value that better fits the numerical results with experimental data. Additionally, we can verify the suitability of the identified properties in describing the material's behavior in other contexts. The simplicity and cost-effectiveness of 2D DIC render it a compelling choice for producing input curves for finite element models, providing a degree of accuracy suitable for most practical scenarios.

Author's Contribuitions: Conceptualization, AS Almeida and CRM Roesler; Methodology, AA Almeida and APG Santos; Investigation, AS Almeida and APG Santos; Writing - original draft, AS Almeida; Writing - review & editing, AS Almeida; CRM Roesler and APG Santos; Funding acquisition, CRM Roesler; Resources, CRM Roesler; Supervision, CRM Roesler and APG Santos.

Data Availability: Research data is not available

Editor: Eduardo Alberto Fancello and Paulo de Tarso Mendonça

References

ABNT, 2013, "ABNT NBR ISO 6892-1 Materiais metálicos - Ensaio de tração. Parte 1: Método de ensaio à temperatura ambiente".

ASTM International, 2022, "ASTM E8/E8M-21 Standard Test Methods for Tension Testing of Metallic Materials", West Conshohocken, PA, www.astm.org.

ASTM International, 2020, "ASTM F2193-20 Standard Specifications and Test Methods for Components Used in the Surgical Fixation of the Spinal Skeletal System", West Conshohocken, PA, www.astm.org.

Berti, F., La Barbera, L., Piovesan, A., Allegretti, D., Ottardi, C., Villa, T., and Pennati, G., 2018, “Residual stresses in titanium spinal rods: effects of two contouring methods and material plastic properties”, Journal of Biomechanical Engineering, 140(11), 111001.

Blaber, J., and Antoniou, A., 2015, “Ncorr Instruction Manual Version 1.2.1”, Georgia Institute of Technology, http://www.ncorr.com/download/ncorrmanual_v1_2_1.pdf.

Bridgman, P. W., 1943, “The stress distribution at the neck of a tension specimen”. Trans. Amer. Soc.

Castro, P. B., 2012, “Identification of constitutive parameters by using full-field measurements”, Doctoral Thesis, Federal University of Santa Catarina.

Gromada, M., Mishuris, G., and Öchsner, A., 2011, “Correction formulae for the stress distribution in round tensile specimens at neck presence”, Springer Science & Business Media.

Le Roy, G., Embury, J. D., Edwards, G., and Ashby, M. F., 1981, “A model of ductile fracture based on the nucleation and growth of voids”, Acta Metallurgic, 29(8), 1509-1522.

Lu, F., Mánik, T., Lægreid Andersen, I., and Holmedal, B., 2021, “A Robust Image Processing Algorithm for Optical-Based Stress–Strain Curve Corrections after Necking”, Journal of Materials Engineering and Performance, 30(6), 4240-4253.

Narayan, R. J., 2012, “ASM Handbook”, Volume 23, Materials for Medical Devices. Materials Park: ASM International.

Pan, B., Xie, H., Wang, Z., Qian, K., and Wang, Z., 2008, “Study on subset size selection in digital image correlation for speckle patterns”, Optics express, 16(10), 7037-7048.

Pinto, O. T., 2014, “Estudo numérico experimental de tecido conjuntivo mole submetido a deformações finitas”, Master Thesis, Federal University of Santa Catarina.

Tu, S., Ren, X., He, J., and Zhang, Z., 2020, “Stress-strain curves of metallic materials and post-necking strain hardening characterization: A review”, Fatigue & Fracture of Engineering Materials & Structures, 43(1), 3-19.

Zhao, J., Sang, Y., and Duan, F., 2019, “The state of the art of two-dimensional digital image correlation computational method”, Engineering reports, 1(2), e12038.